A unified theory of E/I synaptic balance, quasicritical neuronal avalanches and asynchronous irregular spiking

Mauricio Girardi-Schappo[1,2*], Emilio F. Galera[2], Tawan T. A. Carvalho[3], Ludmila Brochini[4], Nilton L. Kamiji[2], Antonio C. Roque[2], Osame Kinouchi[2]

1 Physics Department, STEM Complex, University of Ottawa, Ottawa, ON, K1N 6N5, Canada
2 Departamento de Física, FFCLRP, Universidade de São Paulo, Ribeirão Preto, SP, 14040-901, Brazil
3 Departamento de Física, Universidade Federal de Pernambuco, Recife, PE, 50670-901, Brazil
4 Instituto de Matemática e Estatística, Universidade de São Paulo, São Paulo, SP, 05508-090, Brazil

* girardi.s@gmail.com

Abstract

Neuronal avalanches and asynchronous irregular (AI) firing patterns have been thought to represent distinct frameworks to understand the brain spontaneous activity. The former is typically present in systems where there is a balance between the slow accumulation of tension and its fast dissipation, whereas the latter is accompanied by the balance between synaptic excitation and inhibition (E/I). Here, we develop a new theory of E/I balance that relies on two homeostatic adaptation mechanisms: the short-term depression of inhibition and the spike-dependent threshold increase. First, we turn off the adaptation and show that the so-called static system has a typical critical point commonly attributed to self-organized critical models. Then, we turn on the adaptation and show that the network evolves to a dynamic regime in which: (I) E/I synapses balance regardless of any parameter choice; (II) an AI firing pattern emerges; and (III) neuronal avalanches display visually accurate power laws. This is the first time that these three phenomena appear simultaneously in the same network activity. Thus, we show that the once thought opposing frameworks may be unified into a single dynamics, provided that adaptation mechanisms are in place. In our model, the AI firing pattern is a direct consequence of the hovering close to the critical line where external inputs are compensated by threshold growth, creating synaptic balance for any E/I weight ratio.

Author summary

Two competing frameworks are employed to understand the brain spontaneous activity, both of which are backed by computational and experimental evidence: globally asynchronous and locally irregular (AI) activity arises in excitatory/inhibitory balanced networks subjected to external stimuli, whereas avalanche activity emerge in excitable systems on the critical point between active and inactive states. Here, we develop a new theory for E/I networks and show that there is a state where synaptic balance coexists with AI firing and power-law distributed neuronal avalanches. This regime is achieved

through the introducing of short-time depression of inhibitory synapses and spike-dependent threshold adaptation. Thus, the system self-organizes towards the balance point, such that its AI activity arises from quasicritical fluctuations. The need for two independent adaptive mechanisms explains why different dynamical states are observed in the brain.

Introduction

Self-organized quasicriticality (SOqC), as defined by Bonachela and Muñoz [1], appears in nonconservative models for forest-fires, earthquakes and neuronal networks [2]. The self-organization consists of a local load-dissipation homeostatic mechanism incorporated in a system that has an underlying critical point. In the context of neuroscience, this point is often a second-order absorbing state transition where neuronal avalanches present apparent power law scaling. These adaptive networks frequently include only excitatory neurons, and the homeostatic mechanism is implemented as short-term synaptic depression or, sometimes, as adaptation of the firing probabilities or thresholds of the neurons (see [3, 4] for reviews). Due to the empirical observation of neuronal avalanches [5–7], these models are told to be good representations of the spontaneous activity of the healthy cortex [8].

Alternatively, when inhibitory neurons are included in the model, a globally asynchronous and locally irregular (also known as AI) regime of spontaneous firing emerges (see [9, 10] for reviews). Such activity is generated by a dynamic balance of inhibitory and excitatory inputs to the cells [11], where the net synaptic current tends to remain close to zero. The AI regime usually requires tuning of the parameters of the network, such as the thresholds or the excitatory-inhibitory (E/I) synaptic weight ratio [12]. Although neuronal avalanches were not found in synchronous-irregular (SI) states of E/I networks [13], we showed that synaptic balance may be achieved via the same homeostatic mechanisms that generate a quasicritical state [14]. In addition, E/I networks with weak excitation and inhibition tend to show neuronal avalanches away from the AI regime [15].

Here, we develop the theory of a self-organized E/I network, where inhibition homeostatically adapts according to short-term synaptic depression and thresholds adapt by increasing after each neuronal firing. We derive analytical expressions for the firing rates and compare them to simulations. Interestingly, our network robustly evolves in time towards a state close to the critical point, where: (I) synapses are balanced, (II) the firing pattern is AI; and (III) neuronal avalanches emerge and visually follow a power law. The regime where these three distinct phenomena coexist has never been reported, and they emerge, here, due to the homeostatic adaptation that leads to self-organized quasicritical fluctuations. Specifically, synaptic balance and AI firing pattern occur for any choice of parameters, *i.e.,* regardless of any sort of parameter tuning. Neuronal avalanches that visually obey power laws appear when the homeostatic adaptation time scales are large enough (hundreds to a few thousands of milliseconds, hence ~~experimentally~~ biologically plausible).

We show that ~~the~~ threshold adaptation plays a dominant role when compared to synaptic depression, even when both are subjected to the same time scales. Thus, the self-organized system tends to hover in an AI state where external inputs are dynamically compensated by the spike-dependent thresholds. Without the adaptation in synapses and thresholds, we show that our model presents a typical transition into an absorbing state, causing the different firing patterns (AI, SI, and critical avalanches) to be separated in the phase diagram.

The paper is organized as follows: we introduce the E/I network and the simulation details in the model section; then the mean-field approximation section is used to

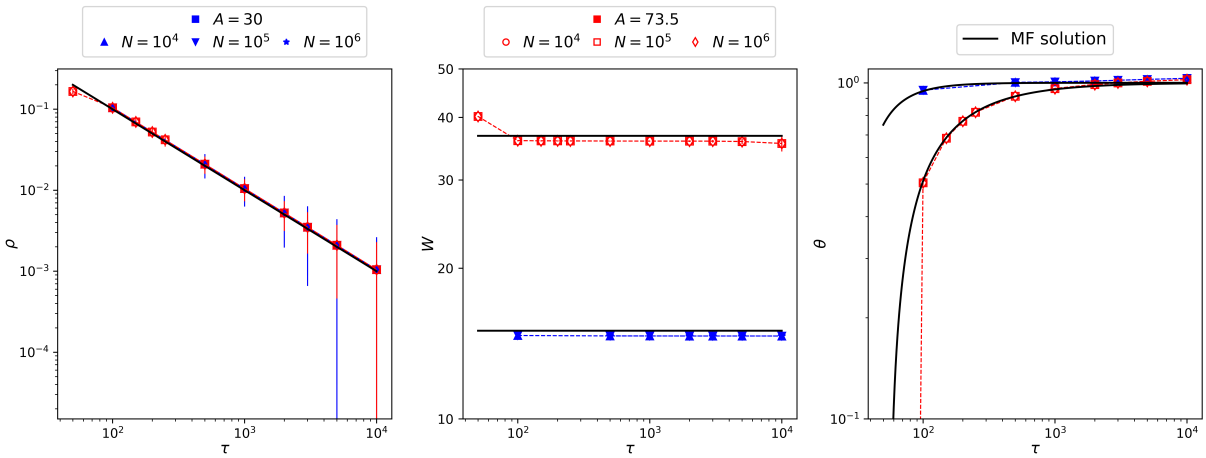

Fig 1. Network stationary activity. Average network activity as a function of $\tau_{w,\theta} = \tau$ compared to the mean-field analytic solution, Eq. (23) as a solid line. We ran simulations in two configurations: fine-tuned to the critical point, $A = A_c = 30$ from Eq. (25) (▲ $\to N = 10^4$, ▼ $\to N = 10^5$, ★ $\to N = 10^6$), and in the supercritical regime, $A = 73.5 > A_c$ (○ $\to N = 10^4$, □ $\to N = 10^5$, ◊ $\to N = 10^6$).

calculate the firing rates, characterize the critical point, and determine the self-organization behavior of the network (both for its firing rates and for its synaptic currents). Finally, we present the neuronal avalanches and scaling of the model and discuss its implications in the last two sections.

The model

We study the excitatory/inhibitory network of [14], where each neuron is a stochastic leaky integrate-and-fire unit with discrete time step equal to 1 ms, connected in an all-to-all graph. A binary variable indicates if the neuron fired ($X[t] = 1$) or not ($X[t] = 0$). The membrane potential of each cell i in either the excitatory (E) or inhibitory (I) population is given by

$$V_i^{E/I}[t+1] = \left[\mu_i V_i^{E/I}[t] + I_i^{\text{ext}}[t] + \frac{1}{N}\sum_{j=1}^{N_E} J_{ij} X_j^E[t] - \frac{1}{N}\sum_{j=1}^{N_I} W_{ij} X_j^I[t]\right]\left(1 - X_i^{E/I}[t]\right), \tag{1}$$

where J_{ij} is the synaptic coupling strength, $W_{ij} = gJ_{ij}$ is the inhibitory coupling strength, g is the inhibition to excitation (E/I) coupling strength ratio, μ is the leak time constant, and $I_i^{\text{ext}}[t]$ is an external current. The total number of neurons in the network is $N = N_E + N_I$, where the fractions of excitatory and inhibitory neurons are kept fixed at $p = N_E/N = 0.8$ and $q = N_I/N = 0.2$, respectively, as reported for cortical data [16] – although the values of p and q do not alter the dynamics of the network [14]. Note that the membrane potential is reset to zero at the $t+1$ instant if a spike occurred at t because of the factor $(1 - X_i^{E/I}[t])$.

All parameters are positively defined and are assumed to be self-averaging (i.e., single-peaked distributions with small coefficients of variation). Letting the excitatory synaptic current be $I_i^E[t] \equiv (1/N)\sum_j J_{ij} X_j^E[t]$ and the inhibitory be $I_i^I[t] \equiv -(1/N)\sum_j W_{ij} X_j^I[t]$, we define the net synaptic current,

$$\Delta I^{E/I}[t] = I^E[t] + I^I[t]\,. \tag{2}$$

Eq. (1) is the same for both excitatory and inhibitory populations. This happens because the inhibitory self-coupling and the inhibitory coupling to the excitatory population are both given by W_{ij}, whereas the self-coupling of the excitatory population and the coupling of the excitatory to the inhibitory population are both given by J_{ij}.

At any time step, a neuron fires according to a piecewise linear sigmoidal probability $\Phi(V)$,

$$\Phi(V) \equiv P\left(X = 1|V\right) = (V - \theta)\Gamma\, \Theta(V - \theta)\, \Theta(V_S - V) + \Theta(V - V_S), \tag{3}$$

where θ is the firing threshold, Γ is the firing gain constant, $V_S = 1/\Gamma + \theta$ is the saturation potential, and $\Theta(x > 0) = 1$ (zero otherwise) is the step function.

This model is known to present a mean-field directed percolation critical point [14, 17] at $g = g_c$, such that $g < g_c$ is the active excitation-dominated (supercritical) phase and $g > g_c$ corresponds to the inhibition-dominated absorbing state (subcritical). The synapses in the critical point g_c are dynamically balanced: fluctuations in excitation are immediately followed by counter fluctuations in inhibition [14].

The critical point g_c may be achieved dynamically by adding inhibitory synaptic depression through

$$W_{ij}[t+1] = W_{ij}[t] + \frac{1}{\tau_w}\left(A - W_{ij}[t]\right) - u_w W_{ij}[t] X_j^I[t]\,, \tag{4}$$

and threshold adaptation,

$$\theta_i[t+1] = \theta_i[t] - \frac{1}{\tau_\theta}\theta_i[t] + u_\theta \theta_i[t] X_i[t]\,. \tag{5}$$

The parameters u_θ and u_W are the fractions of threshold increase and synaptic depression, respectively, τ_θ and τ_W should be moderately large decay time scales and A is a baseline synaptic coupling strength. Instead of inhibition, we can also homeostatically regulate the excitatory synapses [14], J_{ij}, but experimental evidence suggests that it is the inhibitory synapses that tend to adapt to the excitation level of the network, and not the contrary [7, 9].

Simulations

We ran simulations corresponding to Eqs. (1) to (5), and compared them to the analytical results developed in the forthcoming sections. Unles otherwise stated, we fixed the parameters $p = 0.8$ (fraction of excitatory neurons), $q = 0.2$ (fraction of inhibitory neurons), $I^{\text{ext}} = 1$ (external current), $\Gamma = 0.2$ (neuronal firing gain), $\mu = 0$ (leakage inverse time constant), $J = 10$ (excitatory weight), and $u_{w,\theta} = u = 0.1$ (the fraction of inhibition depression and threshold adaptation, respectively). The remaining parameters, N (total number of neurons in the network), τ_w (recovery time constant of the inhibitory synapses), τ_θ (recovery time of the threshold) and A (maximum dynamical inhibition) were systematically explored. Some simulations have $\tau \equiv \tau_w = \tau_\theta$. Fig. 1 shows the average activity of the network simulated as a function of τ for different N, compared to the analytical description derived in the next section.

All simulations were ran for a total of 1,000,000 time steps, and averages were calculated after discarding the first 10,000 time steps to avoid transient effects. We use the conversion factor of 1 time step = 1 millisecond, since a spike of a neuron, here, takes 1 time step.

Mean-field approximation

The mean-field approximation is exact for our complete graph network with self-averaging parameters. Thus, we define the synaptic couplings as $J = \langle J_{ij} \rangle$ and $W = \langle W_{ij} \rangle$ (such that $g = W/J$), $I^{\text{ext}}[t] = \langle I_i^{ext}[t] \rangle$ and $\mu = \langle \mu_i \rangle$, where $\langle . \rangle$ means average over neurons. We also define the firing rates (the fraction of active sites per time step) $\rho_E[t] = 1/N_E \sum_j X_j^E[t]$ and $\rho_I[t] = 1/N_I \sum_j X_j^I[t]$. The fractions of excitatory and inhibitory neurons are $p = N_E/N$ and $q = 1 - p = N_I/N$, respectively. Under these conditions, we can average Eq. (1):

$$V^{E/I}[t+1] = \Big[\mu V^{E/I}[t] + I^{\text{ext}}[t] + pJ\rho_E[t] - qW\rho_I[t]\Big]\Big(1 - \rho_{E/I}[t]\Big) . \tag{6}$$

We may omit the E/I superscripts since this equation holds for both populations.

From the definition of the firing function, $\Phi(V)$ in Eq. (3), the model may have two types of stationary states: the active state, such that the density of active sites is $\rho_E = \rho_I \equiv \rho^* > 0$, and the quiescent state, where $\rho_E = \rho_I \equiv \rho^0 = 0$. At instant $t+1$, the active population is simply given by

$$\rho_{E/I}[t+1] = \int_\theta^\infty \Phi(V)\, P_t^{E/I}(V)\, dV , \tag{7}$$

where $\Phi(V)$ is the conditional probability of firing at $t+1$ given V at t, and $P_t^{E/I}(V)$ is the probability of having a neuron with potential V at time t.

This relation is sufficient for deriving the temporal evolution map for ρ because the reset of the potential causes the k-th subpopulation of neurons that fired together to also evolve together until they fire again. This allows us to write $P_t^{E/I}(V)$ as a sum of subpopulations,

$$P_t^{E/I}(V) = \sum_{k=0}^{\infty} \eta_k^{E/I}[t]\ \delta\left(V - U_k^{E/I}[t]\right) , \tag{8}$$

with $\delta(V)$ the Dirac's delta function and

$$\eta_{k+1}^{E/I}[t+1] = \Big(1 - \Phi(U_k^{E/I}[t])\Big)\, \eta_k^{E/I}[t] , \tag{9}$$

$$U_{k+1}^{E/I}[t+1] = \mu U_k^{E/I}[t] + I^{\text{ext}}[t] + pJ\rho_E[t] - qW\rho_I[t] , \tag{10}$$

where $U_k^{E/I}[t]$ is the membrane potential of the k-th population of excitatory or inhibitory neurons that fired k time steps before t and $\eta_k^{E/I}[t]$ is the proportion of such neurons with respect to the total excitatory or inhibitory population. The potentials U come from Eq. (6), and the $k = 0$ population has $U_0^{E/I}[t] = 0$ for any t, since the reset potential is zero. Then, Eq. (7) is reduced to:

$$\rho_{E/I}[t+1] = \sum_{k=0}^{\infty} \Phi(U_k^{E/I}[t])\, \eta_k^{E/I}[t] . \tag{11}$$

A neuron with firing age k at time t can, at time $t+1$, either fire with probability $\Phi(U_k^{E/I}[t])$ or become part of the population with firing age $k+1$ that has density $\eta_{k+1}^{E/I}[t+1]$.

The stationary state is given by the fixed point of Eq. (11). Inserting Eqs. (9) and (10) into Eq. (11) and assuming that the state of the system at $t+1$ equals the state at

t, we get:

$$\rho = \sum_{k=1}^{\infty} \eta_k \Phi(U_k) \,, \tag{12}$$

$$\eta_k = \eta_{k-1}(1 - \Phi(U_{k-1})) \,, \tag{13}$$

$$U_k = \mu U_{k-1} + \overline{W}\rho + I^{\text{ext}} = (\overline{W}\rho + I^{\text{ext}}) \sum_{n=0}^{k-1} \mu^n = (\overline{W}\rho + I^{\text{ext}}) \frac{1-\mu^k}{1-\mu} \,, \tag{14}$$

where $U_0 = 0$, and we have used $\overline{W} = pJ - qW$ because $\rho_E = \rho_I = \rho$. Plugging Eqs. (13) and (14) into (12) and shifting the sum index yields:

$$\rho = \sum_{k=0}^{\infty} \eta_k (1 - \Phi(U_k)) \Phi(\mu U_k + \overline{W}\rho + I^{\text{ext}}).$$

Considering the case where the stationary potentials lie on the linear part of the firing function, Φ, *i.e.* $\theta < U_1 < \cdots < U_\infty < V_S$, with $U_\infty = (\overline{W}\rho + I^{\text{ext}})/(1-\mu)$ being the limiting potential when $k \to \infty$. Then, using the expression from Eq. (3), we may explicitly write the second $\Phi(V)$ in the previous equation to get

$$\rho = \sum_{k=0}^{\infty} \eta_k (1 - \Phi(U_k)) \, \Gamma \left(\mu U_k + \overline{W}\rho + I^{\text{ext}} - \theta \right) .$$

By using the relation in Eq. (12) and the normalization $\sum_{k=0}^{\infty} \eta_k = 1$, we obtain:

$$\rho = -\Gamma\overline{W}\rho^2 + \left(\mu + \Gamma\overline{W} - \Gamma(I^{\text{ext}} - \theta) \right) \rho + \Gamma h - \Gamma\mu \sum_{k=0}^{\infty} \eta_k \Phi(U_k) U_k \,,$$

where we define $h = I^{\text{ext}} - (1-\mu)\theta$ as the suprathreshold external current, which may be regarded as an external field. Using equation (14) to describe U_k only outside of the Φ function argument in the sum of the last term, leads to:

$$\frac{\Gamma\overline{W}}{1-\mu}\rho^2 + \left(1 - \mu + \frac{\Gamma h}{1-\mu} - \Gamma\overline{W} \right) \rho - \Gamma h - \frac{\mu(\overline{W}\rho + I^{\text{ext}})}{1-\mu} \sum_{k=0}^{\infty} \eta_k \Phi(U_k) \mu^k = 0 \,, \tag{15}$$

that holds when all stationary potentials lie in the linear region of the Φ function, i.e., when $U_1 > \theta$ and $U_\infty < V_S$.

Critical exponents without homeostasis

The leakage of the cells should not be instantaneous, but rather happen in the time scale given by $1/\mu$. Hence, it is reasonable that $0 \leq \mu \leq 1$ is the important range for the dynamics of the network. Within this range, the sum in Eq. (15) converges to zero close to the critical point $\overline{W}_c$, or whenever the network lies in a silent regime (zero firings in average). This happens because, when in silence, the firing rate of the network $\rho = \sum_k \eta_k \Phi(U_k) \to 0$ (which holds arbitrarily close to $\overline{W}_c$ as well), and $\eta_k \Phi(U_k) \mu^k \leq \eta_k \Phi(U_k)$ for $k \geq 0$, resulting in the mean-field equation for the order parameter:

$$\frac{\Gamma\overline{W}}{1-\mu}\rho^2 + \left(1 - \mu + \frac{\Gamma h}{1-\mu} - \Gamma\overline{W} \right) \rho - \Gamma h = 0 \,. \tag{16}$$

The critical point lies on the null external field, $h = h_c = 0$, yielding the stationary solution to Eq. (16), also known as the order parameter,

$$\rho = \frac{\overline{W} - \overline{W}_c}{\overline{W}} (1-\mu) \sim (\overline{W} - \overline{W}_c)^\beta \,, \tag{17}$$

with $\beta = 1$ being its corresponding critical exponent, and

$$\overline{W}_c = \frac{1-\mu}{\Gamma} \,. \tag{18}$$

These relations can also be written in terms of the synaptic coupling ratio, $g = W/J$, as:

$$\rho = \frac{g - g_c}{g - p/q}(1-\mu) \,, \qquad g_c = \frac{p}{q} - \frac{1-\mu}{q\Gamma J} \,. \tag{19}$$

For $\mu = 0$, the expression for g_c reduces to the one obtained previously in Ref. [14].

The field exponent is obtained by isolating h in Eq. (16), taking $\overline{W} = \overline{W}_c$, and expanding for small ρ,

$$h = \frac{(1-\mu)\rho^2}{(1-\mu-\rho)\Gamma} \sim \frac{\rho^{\delta_h}}{\Gamma} \,, \tag{20}$$

with $\delta_h = 2$. The susceptibility exponent, $\chi = \partial\rho/\partial h|_{h=0}$, is obtained by differentiating Eq. (16):

$$\chi = \left.\frac{\partial \rho}{\partial h}\right|_{h=0} = \frac{\overline{W}_c(1-\mu+\Gamma\overline{W}) - (1-\mu)\overline{W}}{\overline{W}(\overline{W}-\overline{W}_c)(1-\mu)} \sim (\overline{W}-\overline{W}_c)^{-\gamma} \,, \tag{21}$$

with $\gamma = 1$. This value, together with $\beta = 1$ and $\delta_h = 2$ puts this model into the mean-field directed percolation (MF-DP) universality class [18,19]. Thus, having $0 < \mu < 1$ does not change the nature of the phase transition undergone by the E/I network, as expected [14,17,20].

Is the homeostatic stationary state quasicritical?

We will derive a mean-field map for the dynamics of the network subjected to homeostatic synaptic inhibition and threshold adaptation. Many studies have shown that a single homeostatic dynamics leads to hovering around the critical point [21–25]. Here, we investigate in detail whether two independent homeostatic dynamics are able to do the same. The discussion in this section is systematically explored in terms of the phase diagrams of the E/I network in Fig. 2.

Since μ does not change the critical exponents, we take $\mu = 0$ for simplicity, such that all the subpopulations $k \geq 1$ have the same membrane potential: from Eq. (10), $U_{k+1}[t] = U_k[t] = U_1[t]$ (recall that $U_0 = 0$). This reduces the probability in Eq. (8) to $P_t(V) = \rho[t]\delta(V) + (1-\rho[t])\,\delta(V - U_1[t])$. Note that now there are only two subpopulations: the neurons that fired at time t, corresponding to $\eta_0[t] = \rho[t]$, and the neurons that did not fire, yielding $\eta_1[t] = 1 - \rho[t]$ from the normalization condition $\sum_k \eta_k[t] = 1$.Using this probability in Eq. (7) and averaging Eqs. (4) and (5) over sites, we obtain the following 3-dimensional mean-field map:

$$\begin{aligned} \rho[t+1] &= (1-\rho[t])\,\Gamma\left(pJ\rho[t] - qW[t]\rho[t] + I^{\text{ext}} - \theta[t]\right) \,, \\ W[t+1] &= W[t] + \frac{1}{\tau_w}\left(A - W[t]\right) - u_w W[t]\rho[t] \,, \\ \theta[t+1] &= \theta[t] - \frac{1}{\tau_\theta}\theta[t] + u_\theta \theta[t]\rho[t] \,. \end{aligned} \tag{22}$$

Here, we are only interested in the solutions with $\rho > 0$, since we used only the linear part of the Φ function to derive the $\rho[t]$ map in Eq. (22). The stationary state of the mean-field map is given by the fixed point $(\rho^*, W^*, \theta^*) = (\rho[t+1], W[t+1], \theta[t+1]) = (\rho[t], W[t], \theta[t])$ and yields two different

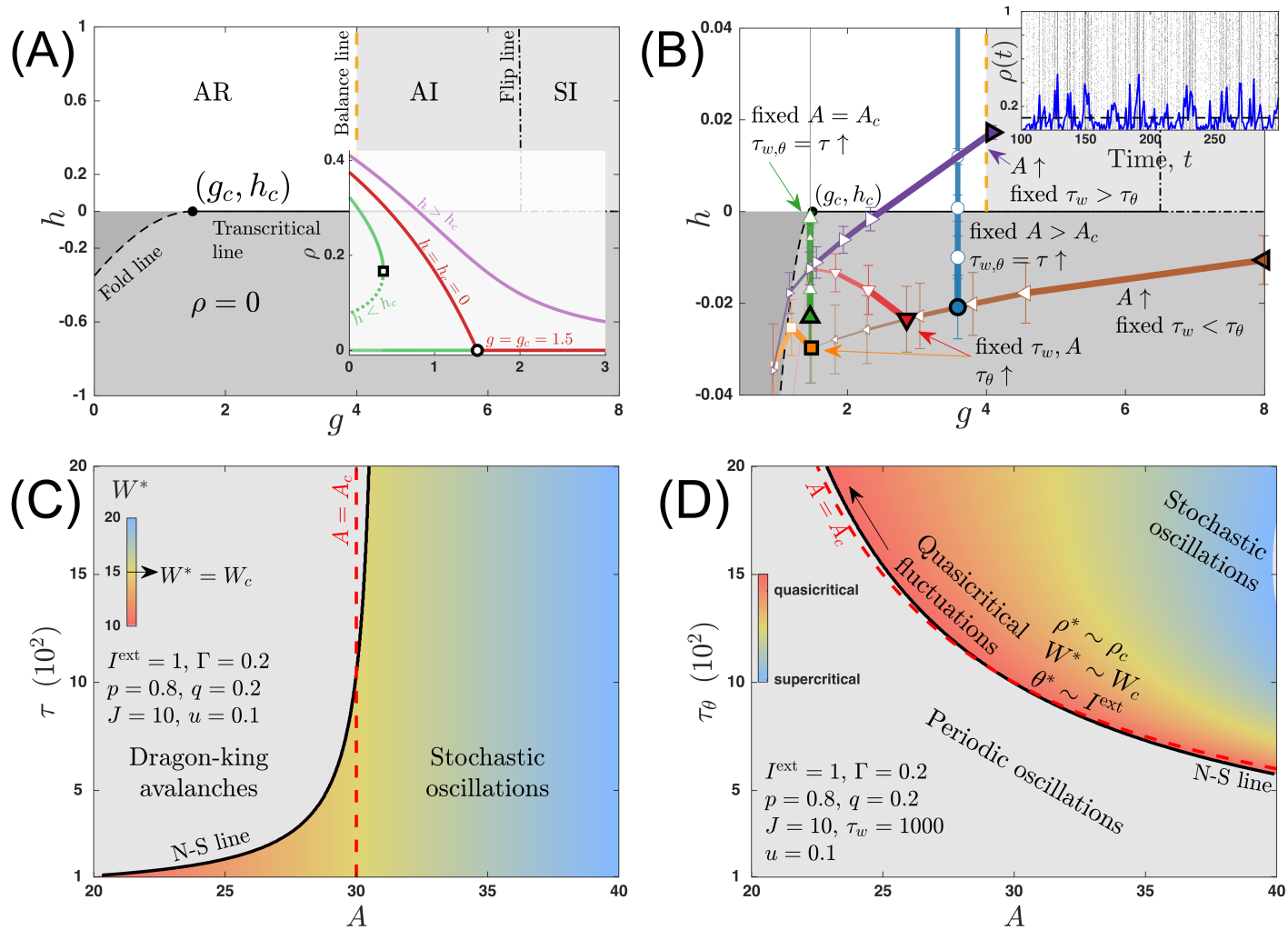

Fig 2. Phase diagrams of the E/I network. (A) Phase diagram derived from the bifurcations of the model without self-organization (constant W and θ), represented by Eq. (16). At $h = h_c = I^{\text{ext}} - \theta_c = 0$, the model undergoes a continuous phase transition of the MF-DP type for $g = g_c = W_c/J = 1.5$. For $h > h_c$, three typical firing patterns appear: asynchronous regular (AR), asynchronous irregular (AI), and synchronous irregular (SI) [14]. **(B)** Stationary states of the homeostatic model localized over the phase diagram of the static model in panel A (i.e., here W and θ evolve according to Eqs. (4) and (5), respectively). Each marker corresponds to the stationary state of the homeostatic E/I network for a different configuration of A, τ_θ and τ_w, whereas the size of the marker and the thickness of the line indicate the direction of growth of the control parameter as follows: $\circ \rightarrow$ fixed $A = 73.5 > A_c$, controlling for $\tau_{w,\theta} = \tau$; $\triangle \rightarrow$ fixed $A = A_c = 30$, controlling for $\tau_{w,\theta} = \tau$; $\triangledown \rightarrow$ fixed $A = 37.5$ and $\tau_w = 3000$, controlling for τ_θ; $\square \rightarrow$ fixed $A = 19.5$ and $\tau_w = 3000$, controlling for τ_θ; $\triangleleft \rightarrow$ fixed $\tau_w = 3000$ and $\tau_\theta = 2000$, controlling for A; $\triangleright \rightarrow$ fixed $\tau_w = 3000$ and $\tau_\theta = 10000$, controlling for A. The largest value of the control parameter is indicated by a marker with a black contour. Any of the considered configurations render the system within 4% of h_c. However, different configurations vary widely on the g axis, remaining very close to g_c only for $A = A_c$, Eq. (25). **(B), inset,** the typical activity of the homeostatic system in many configurations is AI (aperiodic fluctuating average with microscopic irregular firing, shown in the background raster plot). **(C) and (D)** Phase diagrams of the homeostatic model in the plane $\tau_{w,\theta} = \tau$ vs. A (C) and τ_θ vs. A for fixed $\tau_w = 1000$ (D). The solid line marks a numerically determined subcritical Neimark-Sacker (N-S) bifurcation from the fixed point (colored region), whereas the dashed line highlights the fine-tune, $A = A_c$. For large enough τ_θ, the critical line A_c is close to the N-S bifurcation. Critical fluctuations, where the three variables, $\rho[t]$, $W[t]$ and $\theta[t]$, remain close to (ρ_c, W_c, θ_c), are only found in the vicinity of the A_c line. Dragon-kings (large avalanches) and periodic oscillations are present in the empty grey areas.

types of solutions: the stable dynamics (when $\theta > 0$),

$$\begin{aligned}
\rho^* &= \frac{1}{u_\theta \tau_\theta} \\
W^* &= \frac{A}{1 + \frac{u_w \tau_w}{u_\theta \tau_\theta}} \\
\theta^* &= I^{\text{ext}} + \frac{pJ}{u_\theta \tau_\theta} - \frac{qA}{u_\theta \tau_\theta + u_w \tau_w} + \frac{1}{(1 - u_\theta \tau_\theta)\Gamma}
\end{aligned} \tag{23}$$

and the unstable hyper-excited state ($\theta = 0$). The stability of the asymptotic solutions was numerically checked.

The critical point of the underlying system that we want to dynamically reach is given by $\overline{W}_c = pJ - qW_c = 1/\Gamma$ and $h_c = I^{\text{ext}} - \theta_c = 0$, which yields:

$$\begin{aligned}
\rho_c &= 0 \,, \\
W_c &= \frac{p}{q} J - \frac{1}{q\Gamma} \,, \\
\theta_c &= I^{\text{ext}} \,.
\end{aligned} \tag{24}$$

From Eq. (23), we see that taking fixed $u_{\theta,w}$ and τ_w with $u_\theta \tau_\theta \gg 1$ is enough to achieve

$$\begin{aligned}
\rho^* &\sim \rho_c = 0 + \mathcal{O}\left[1/\tau_\theta\right] \,, \\
\theta^* &\sim \theta_c = I^{\text{ext}} + \mathcal{O}\left[1/\tau_\theta\right] \,,
\end{aligned}$$

but that would still leave us with

$$W^* \sim A + \mathcal{O}\left[1/\tau_\theta\right] \,,$$

when $\tau_\theta \neq \tau_w$, or

$$W^* = \frac{A}{1 + u_w/u_\theta} \,,$$

when both homeostatic dynamics have equal time constants.

Therefore, to meet the last requirement for reaching the critical point, $W^* \sim W_c$, we still need to fine-tune the parameter $A = A_c$, with

$$A_c = \frac{pJ\Gamma - 1}{q\Gamma} \left(1 + \frac{u_w \tau_w}{u_\theta \tau_\theta}\right) \,. \tag{25}$$

To understand why the fine-tuning is necessary, it is useful to isolate W^* from the $\rho[t]$ map in Eq. (22), using $\rho^* = 1/(u_\theta \tau_\theta)$,

$$\begin{aligned}
W^* &= \frac{p}{q} J - \frac{1}{q\Gamma} \frac{1}{1 - \frac{1}{u_\theta \tau_\theta}} - \frac{u_\theta \tau_\theta}{q} (\theta^* - I^{\text{ext}}) \\
W^* &\sim W_c - \frac{u_\theta \tau_\theta}{q} (\theta^* - I^{\text{ext}}) + \mathcal{O}\left[1/\tau_\theta^2\right] \,.
\end{aligned} \tag{26}$$

Since $\theta^* - I^{\text{ext}} \sim \mathcal{O}\left[1/\tau_\theta\right]$, the last term in Eq. (26) is of $\mathcal{O}\left[1\right]$, resulting in a displacement from the critical point along the $g = W^*/J$ axis that is independent of τ_θ (see Fig. 2).

Although the requirements upon ρ^* and θ^* are met through quasicritical fluctuations, the system still requires fine-tuning on the inhibitory synaptic amplitude. If $\theta^* - I^{\text{ext}} \sim \mathcal{O}\left[1/\tau_\theta^2\right]$, then all the requirements of homeostatic criticality would be met. Hence, the two homeostatic dynamics are canceling each other out, mutually working together to avoid the complete dynamical reach of the critical point.

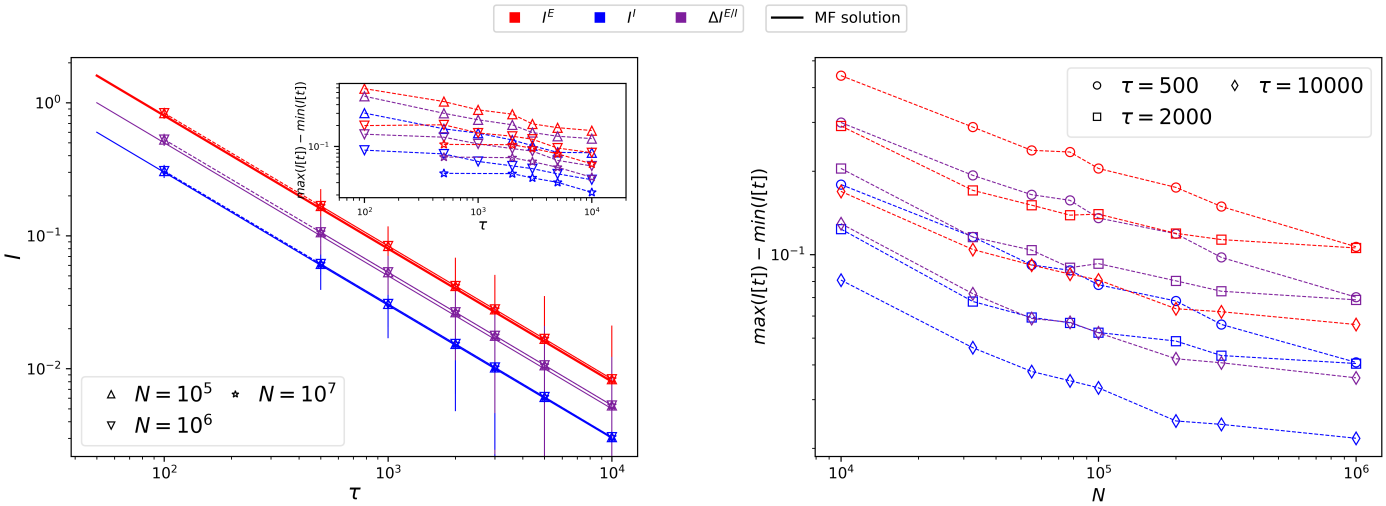

Fig 3. Synaptic currents. (A) Stationary value of the synaptic currents and their maximum amplitudes (inset) as a function of $\tau_{w,\theta} = \tau$. Both tend to zero as τ grows, and the stationary currents follow Eq. (27). **(B)** The maximum amplitude of the synaptic currents decays as the total number of neurons in the network grows. Symbols are simulation results and solid lines are the analytical calculations.

Is the homeostatic stationary state balanced?

The net synaptic current is given by Eq. (2). In the mean-field stationary state, we have the excitatory current $I^E = pJ\rho^*$, and the inhibitory one, $I^I = -qW^*\rho^*$, where ρ^* and W^* are given by Eq. (23), resulting in the net contribution

$$\begin{aligned} \Delta I^{E/I} &= I^E + I^I = \frac{pJ}{u_\theta \tau_\theta} - \frac{qA}{u_\theta \tau_\theta + u_w \tau_w} \\ \Delta I^{E/I} &\sim 0 + \mathcal{O}\left[1/\tau_\theta\right] , \end{aligned} \tag{27}$$

for fixed $u_{\theta,w}$ and τ_w, with $u_\theta \tau_\theta \gg 1$. The absolute values of these currents, I^E, I^I and $\Delta I^{E/I}$, together with their maximum amplitude, is shown in Fig. 3.

This shows that the homeostatic system is balanced up to $\mathcal{O}\left[1/\tau_\theta\right]$. This means that although we may have different ratios of E/I currents (as expressed by A/J), and different regimes of stationary activity, as evidenced in Fig. 2, the system will still manage to dynamically balance its synaptic currents due to the homeostatic mechanisms.

Avalanches and scaling

In this section, we are not interested in thoroughly characterizing the statistics of avalanche distributions, since we already determined that the homeostatic dynamics are able to lead the system into hovering around the critical point under certain conditions. We are only interested in exploring whether power laws can be visually perceived in the system dynamics.

The homeostatic network activity is always slightly supercritical, since $\rho^* \sim 0 + \mathcal{O}\left[1/\tau_\theta\right]$ – a condition that does not generate any absolute period of silence in the total firings of the network. Then, we cannot define the traditional absorbing state avalanches (i.e., setting the network into an absorbing state and seeding it from a single neuron, subsequently waiting for the activity to dissipate back into some absorbing

state [20]). To overcome this issue, we adapt the time series thresholding method described by Villegas *et al.* [26], and apply it to the fluctuations of $\rho[t]$.

The simulation consists of the numerical solution of Eqs. (1) to (5), so we first define the total number of firings per time step, $\eta[t] = N\rho[t] = \sum_1^N X_i[t]$, where $X_i[t]$ indicates a firing of neuron i at instant t (in any of the E/I populations). Then, we choose the threshold $\eta_{\text{th}} = \alpha(\max_t \eta[t] - \min_t \eta[t])$, where we take $\alpha = 0.2$ as the fraction of the activity to be discarded. The results presented here are robust for a wide range of α values, provided that α is neither too close to zero nor to one. Then, we calculate the avalanches using the new time series, $\eta'[t] = \eta[t] - \eta_{\text{th}}$: an avalanche of size S_k and duration T_k is defined as

$$S_k = \sum_{t=t_k}^{t_{k+1}} \eta'[t] \,, \quad T_k = t_{k+1} - t_k \,,$$

where t_k and t_{k+1} are two consecutive moments of silence, i.e. $\eta'[t_k] = \eta'[t_{k+1}] = 0$ and $\eta'[t]|_{t=t_k}^{t_{k+1}} > 0$. This method generates consistent scaling between $\langle S \rangle$ and T in the Ornstein-Uhlenbeck process [26]. The distributions of avalanche size and duration, as well as the scaling $\langle S \rangle (T)$, are plotted in Fig. 4.

The stationary state of our E/I network with constant W and θ presents avalanche scaling that is consistent with absorbing state MF-DP systems [14], namely $P(S) \sim S^{-3/2}$, $P(T) \sim T^{-2}$ and $\langle S \rangle \sim T^2$. The addition of the homeostatic mechanisms creates a peak for very large (and very long) avalanches in $P(S)$ and $P(T)$, and makes the expected scaling of $\langle S \rangle$ vs. T inconsistent with the MF-DP theory. However, both of the distributions still present a visual power-law within a limited range of S and T that is consistent with the expected exponents 3/2 and 2, respectively, provided that $\tau_{w,\theta} = \tau$ is large ($\gtrsim 5000$) and the network has about $N \sim 10^5$ neurons (four panels on the top-right of Fig. 4).

Beyond avalanche distributions, we also checked for the distribution $P(\rho)$, since it is a direct measure of the network activity. Although not standard, at the MF-DP critical point, it can be shown that the expected distribution of the activity follows $P_{DP}(\rho) \sim \rho^{-1/\alpha}$, where $\alpha = 1$ is the critical exponent related to the temporal decay of the activity, $\rho \sim t^{-\alpha}$ [19]. Our model without homeostasis falls into MF-DP, hence it presents this expected scaling at $g = g_c$ (see Fig. 5A, inset). After θ and W are allowed to homeostatically self-organize, the distribution of activity changes its exponent, but still follows a power law $P(\rho) \sim \rho^{-2/3}$ both at $A = A_c$ and $A > A_c$ – a reminiscent evidence of the SOqC dynamics.

Discussion

E/I networks are widely used as a theoretical model to understand neuronal activity: from memory dynamics in the healthy brain [27] to seizure development in epilepsy [28]. Amidst of that, there is an ongoing debate on the statistical features of the spontaneous activity of neuronal networks: should the network present asynchronous and irregular (AI) firing, or should it display neuronal avalanches in the form of activity bursts? Could both of these firing behaviors be reconciled? – In this paper, we offer a detailed theoretical study of a model that brings together both of these ideas: the quasicritical state (generated by the homeostatic mechanisms of synaptic depression and threshold adaptation) presents an AI firing pattern that is typical of E/I networks [14] (also, see Fig. 2B, inset). Namely, the average activity fluctuates without a known periodicity, whereas the microscopic firing of neurons is irregular (any given neuron stochastically fires over time).

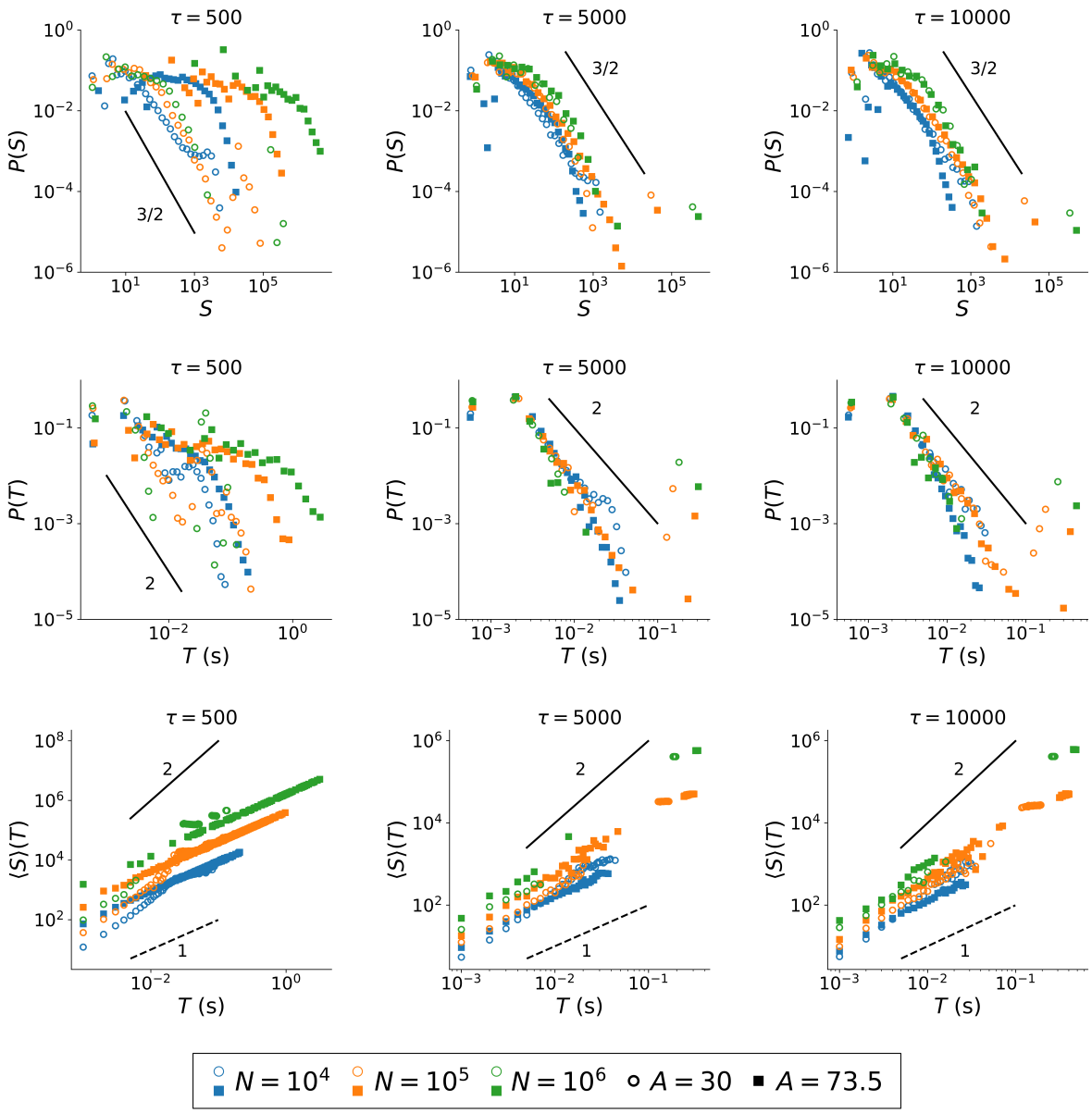

Fig 4. Avalanche distributions and scaling. The distribution of avalanche sizes (S, top row) and duration (T, middle row), together with the scaling relation between size and duration (bottom row), for increasing $\tau_{w,\theta} = \tau$ from left to right. Open circles correspond to the homeostatic system fine-tuned to $A = A_c = 30$, Eq. (25), whereas filled squares correspond to $A = 73.5 > A_c$. Different colors correspond to different N. Solid lines are the power laws of the static system (MF-DP) for visual comparison only, $P(S) \sim S^{-3/2}$, $P(T) \sim T^{-2}$, and $\langle S \rangle \sim T^2$. As τ and N increase, avalanche distributions for both values of A display a limited power-law regime that approach the MF-DP exponents. However, the system display huge avalanches (also known as Dragon-Kings) even when $A = A_c$, independently of τ and N. The scaling law $\langle S \rangle \sim T^2$ is not obeyed (it is best fit by a linear relation instead, dashed line). The huge avalanches and lack of scaling might be due to the method we use to sample of the avalanches (thresholding the time series of the total network activity – see Section on Avalanches and Scaling for details).

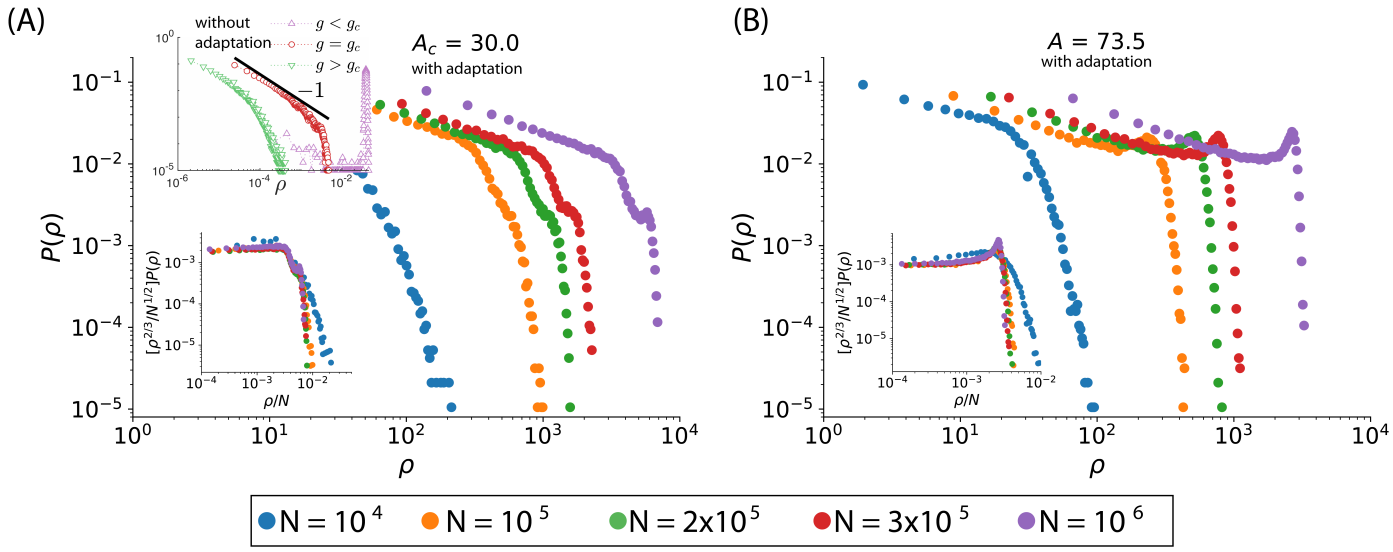

Fig 5. Distribution of activity. (A) Histogram of $\rho[t]$ with self-organization (main panel) and without (top inset). Without self-organization, $P_{DP}(\rho) \sim \rho^{-1}$ is expected from the theory of MF-DP and is found only on the critical point. Bottom inset: collapse of the data in the main panel, showing a scaling exponent $P(\rho) \sim \rho^{-2/3}$ for the homeostatic model at $A = A_c$. **(B)** The histogram of $P(\rho)$ for $A > A_c$ shows the same scaling as in panel A, but now a prominent supercritical peak can be seen at the tail of the distribution.

In addition, we showed that our homeostatic model displays avalanches that have size and duration distributed consistently with the expected MF-DP exponents ($-3/2$ for size and -2 for duration). There are two caveats here: first, we did not thoroughly checked for the correspondence of $P(S)$ and $P(T)$ with power laws through maximum likelihood methods. This is because we know, from the theory that we developed here, that our system hovers close to the critical line where $\theta^* \sim \theta_c$ for moderately large τ_θ; As we showed, by choosing A we may select the global activity through the homeostatic dynamics of W on top of the underlying phase diagram (Fig. 2B), although A does not alter the visual power-law shape of avalanche distributions (Fig. 4) nor the scaling of the activity distribution (Fig. 5). Secondly, the MF-DP scaling, $\langle S \rangle \sim T^{-2}$, is not obeyed by our homeostatic model. Again, this is just a direct consequence of the self-organization mechanism: the homeostatic dynamics is only enough to generate stochastic hovering around the critical line, but the system is never localized exactly at the critical point – the only spot in which the scaling must hold.

Looking for power laws in avalanche distributions is not the most reliable way of looking for a critical point. In absorbing state systems, such as branching processes, the theory gives us many other functions that are potentially observable (see [19], Table 4.1). Here, we proposed to check for a power law in the distribution of the raw firing rate density of the network, $P(\rho)$. Notwithstanding, although our model is theoretically bounded to be near-critical, its avalanche distributions show peaks typical of dragon-king events.

The homeostatic adaptation of inhibitory synapses is inspired by experimental evidence [7, 9]. And here, together with threshold adaptation, it makes our network to always generate synaptic balance (to the $\mathcal{O}[1/\tau_\theta]$), independently of any of the parameters of the model. This is another unifying aspect of our theory, since the balance happens concomitantly with the self-organized quasicritical fluctuations, where the model is visually consistent with complex activity patterns, expressed by the power law distributions of the activity (both for ρ and for S and T).

Interestingly, this is the first time we know of in which two independent homeostatic dynamics are shown to compete and, ultimately, cancel each other. Previous attempts of self-organization mainly focused on the adaptation of synapses (see [3, 4] for reviews). In this case, these systems also require tuning of parameters that are analogous to A in our model [2]. The extra adaptation mechanism presented here, given by threshold increments after each spike, makes our model more robust to changes in A when comparing activity distributions. However, the threshold dominates the dynamics of our network and prevents a complete self-organization towards (ρ_c, W_c, θ_c), since $W^* - W_c \sim \tau_\theta(\theta^* - \theta_c)$ and $\theta^* - \theta_c \sim \mathcal{O}\left[1/\tau_\theta\right]$. By letting A obey another adaptive mechanism, a phenomenon known as metaplasticity [29], we could potentially circumvent the need for tuning. Other solutions could involve having threshold adaptation that yield $\theta^* - \theta_c \sim \mathcal{O}\left[1/\tau_\theta^2\right]$, or altering the firing function, $\Phi(V)$, such that we get an equation for ρ that depends on W and θ through different types of nonlinearities.

The quest put forward by the brain criticality hypothesis continues. Our model displays synaptic balance (independently of parameters) with AI firing patterns, under a two-variables self-organizing dynamic that drives the system close to the critical field, $h_c = 0$; At the same time that his seemingly stochastic AI happens, the activity is complex: neuronal avalanches and firing rates are distributed according to power laws – a reminiscent signature of the criticality that underlies adaptation mechanism. These features are typical of different fields in theoretical neuroscience, and our model is, then, a step towards putting these different frameworks together.

Acknowledgments

This article was produced as part of the S. Paulo Research Foundation (FAPESP) Research, Innovation and Dissemination Center for Neuromathematics (CEPID NeuroMat, Grant No. 2013/07699-0). The authors also thank FAPESP support through Grants No. 2015/50122-0 (A.C.R.), 2016/03855-5 (N.L.K.), 2016/24676-1 (L.B.), 2018/09150-9 (M.G.-S.), 2018/20277-0 (A.C.R.), and 2019/12746-3 (O.K). A.C.R. thanks financial support from the National Council of Scientific and Technological Development (CNPq), Grant No. 306251/2014-0. O.K. thanks the Center for Natural and Artificial Information Processing Systems (CNAIPS)-USP.

References

1. Bonachela JA, Muñoz MA. Self-organization without conservation: true or just apparent scale-invariance? J Stat Mech. 2009; p. P09009.

2. Bonachela JA, de Franciscis S, Torres JJ, Muñoz MA. Self-organization without conservation: are neuronal avalanches generically critical? J Stat Mech. 2010; p. P02015.

3. Kinouchi O, Pazzini R, Copelli M. Mechanisms of self-organized quasicriticality in neuronal networks models. arXiv. 2020;cond-mat.dis-nn:2010.10622.

4. Zeraati R, Priesemann V, Levina A. Self-organization toward criticality by synaptic plasticity. arXiv. 2020;q-bio.NC:2010.07888.

5. Beggs JM, Plenz D. Neuronal avalanches in neocortical circuits. J Neurosci. 2003;23(35):11167–11177.

6. Fontenele AJ, de Vasconcelos NAP, Feliciano T, Aguiar LAA, Soares-Cunha C, Coimbra B, et al. Criticality between Cortical States. Phys Rev Lett. 2019;122:208101. doi:10.1103/PhysRevLett.122.208101.

7. Ma Z, Turrigiano GG, Wessel R, Hengen KB. Cortical Circuit Dynamics Are Homeostatically Tuned to Criticality In Vivo. Neuron. 2019;104(4):655–664.E4. doi:10.1016/j.neuron.2019.08.031.

8. Carvalho TTA, Fontenele AJ, Girardi-Schappo M, Feliciano T, Aguiar LAA, Silva TPL, et al. Subsampled directed-percolation models explain scaling relations experimentally observed in the brain. arXiv. 2020;q-bio.NC:2007.13813.

9. Denève S, Machens CK. Efficient codes and balanced networks. Nat Neurosci. 2016;19:375–382. doi:10.1038/nn.4243.

10. Ahmadian Y, Miller KD. What is the dynamical regime of cerebral cortex? arXiv:190810101v2 [q-bioNC]. 2019;.

11. van Vreeswijk C, Sompolinsky H. Chaos in neuronal networks with balanced excitatory and inhibitory activity. Science. 1996;274(5293):1724–1726.

12. Brunel N. Dynamics of sparsely connected networks of excitatory and inhibitory spiking neurons. J Comput Neurosci. 2000;8(3):183–208.

13. Touboul J, Destexhe A. Power-law statistics and universal scaling in the absence of criticality. Phys Rev E. 2017;95:012413. doi:10.1103/PhysRevE.95.012413.

14. Girardi-Schappo M, Brochini L, Costa AA, Carvalho TTA, Kinouchi O. Synaptic balance due to homeostatically self-organized quasicritical dynamics. Phys Rev Research. 2020;2:012042(R). doi:10.1103/PhysRevResearch.2.012042.

15. Li J, Shew WL. Tuning network dynamics from criticality to an asynchronous state. PLOS Computational Biology. 2020;16:1–16. doi:10.1371/journal.pcbi.1008268.

16. Somogyi P, Tamás G, Lujan R, Buhl EH. Salient features of synaptic organisation in the cerebral cortex. Brain Res Rev. 1998;26:113–135. doi:10.1016/S0165-0173(97)00061-1.

17. Girardi-Schappo M, Tragtenberg MHR. Comment on "Convergence towards asymptotic state in 1-D mappings: A scaling investigation". Phys Lett A. 2019;383(36):126031. doi:10.1016/j.physleta.2019.126031.

18. Muñoz MA, Dickman R, Vespignani A, Zapperi S. Avalanche and spreading exponents in systems with absorbing states. Phys Rev E. 1999;59(5):6175.

19. Henkel M, Hinrichsen H, Lübeck S. Non-Equilibrium Phase Transitions. Dordrecht, The Netherlands: Springer; 2008.

20. Girardi-Schappo M, Tragtenberg MHR. Measuring neuronal avalanches in disordered systems with absorbing states. Phys Rev E. 2018;97:042415. doi:10.1103/PhysRevE.97.042415.

21. Costa AA, Copelli M, Kinouchi O. Can dynamical synapses produce true self-organized criticality? J Stat Mech. 2015;2015(6):P06004.

22. Brochini L, Costa AA, Abadi M, Roque AC, Stolfi J, Kinouchi O. Phase transitions and self-organized criticality in networks of stochastic spiking neurons. Sci Rep. 2016;6:35831.

23. Costa AA, Brochini L, Kinouchi O. Self-Organized supercriticality and oscillations in networks of stochastic Spiking Neurons. Entropy. 2017;19(8):399.

24. Costa AA, Amon MJ, Sporns O, Favela LH. Fractal analyses of networks of integrate-and-fire stochastic spiking neurons. In: International Workshop on Complex Networks. Springer; 2018. p. 161–171.

25. Kinouchi O, Brochini L, Costa AA, Campos JGF, Copelli M. Stochastic oscillations and dragon king avalanches in self-organized quasi-critical systems. Sci Rep. 2019;9:3874.

26. Villegas P, di Santo S, Burioni R, Muñoz MA. Time-series thresholding and the definition of avalanche size. Phys Rev E. 2019;100:012133. doi:10.1103/PhysRevE.100.012133.

27. Vogels TP, Sprekeler H, Zenke F, Clopath C, Gerstner W. Inhibitory plasticity balances excitation and inhibition in sensory pathways and memory networks. Science. 2011;334(6062):1569–1573.

28. Rich S, Hutt A, Skinner FK, Valiante TA, Lefebvre J. Neurostimulation stabilizes spiking neural networks by disrupting seizure-like oscillatory transitions. Sci Rep. 2020;10:15408. doi:10.1038/s41598-020-72335-6.

29. Peng J, Beggs JM. Attaining and maintaining criticality in a neuronal network model. Physica A: Statistical Mechanics and its Applications. 2013;392(7):1611–1620.